Journal Name

Dynamic Article Links ▶

Cite this: DOI: 10.1039/c0xx00000x

www.rsc.org/xxxxxx

ARTICLE TYPE

**†Electronic Supplementary Information (ESI†)**

# Coaxial PANI/TiN/PANI Nanotube Arrays for High-Performance Supercapacitor Electrodes

**Xiang Peng,[b] Kaifu Huo*[a, b], Jijiang Fu,[b] Xuming Zhang,[a] Biao Gao,[b] and Paul K. Chu*[a]**

***Received (in XXX, XXX) Xth XXXXXXXXX 20XX, Accepted Xth XXXXXXXXX 20XX***
**DOI: 10.1039/b000000x**

[a] *Department of Physics and Materials Science, City University of Hong Kong, Tat Chee Avenue, Kowloon, Hong Kong, China. E-mail: paul.chu@cityu.edu.hk*

[b] *School of Materials and Metallurgy, Wuhan University of Science and Technology, Wuhan 430081, China. E-mail: kfhuo@hust.edu.cn*

## Experimental Details

### Fabrication of $TiO_2$, TiN, and PANI/TiN/TiN NTAs

The Ti foils were polished by SiC sandpapers and ultrasonically cleaned with acetone, ethanol, and deionized water sequentially. Anodization was carried out using a conventional two-electrode cell equipped with a direct current (DC) power supply (IT6834, ITECH, China). The Ti and graphite foils served as the anode and counter electrode, respectively (1 cm separation). The electrolyte was composed of ethylene glycol containing 0.5 wt% ammonium fluoride ($NH_4F$), 5 vol% distilled (DI) water and 5 vol% methanol ($CH_3OH$). After anodization at 60 V for 4 h, amorphous $TiO_2$-NTAs were formed on the Ti foils. The samples were ultrasonically cleaned and annealed at 450 $^oC$ in air for 3 h to convert the amorphous $TiO_2$-NTAs into anatase $TiO_2$-NTAs. They were further annealed in $NH_3$ at 750 $^oC$ for 3 h to form the TiN-NTAs.

Electrochemical polymerization of PANI on the TiN-NTAs was performed in a $H_2SO_4$-aniline solution (containing 0.5M $H_2SO_4$ and 0.05M aniline) by cyclicvoltammetry in the potential range of -0.6V to 1 V with a saturated calomel electrode (SCE) as the reference electrode, Pt foil as the counter electrode, and TiN-NTAs as the working electrode. The $H_2SO_4$-aniline solution was ultrasonically treated for 1 min to convert the aniline monomer into nanotubes. Electrochemical deposition was performed for 5, 15, and 30 cycles to achieve different mass loadings on the TiN-NTAs.

### Morphology, structure and composition

The samples were characterized by X-ray diffraction (XRD, Philips X' Pert Pro) with Cu Kα radiation (1.5416 Å) between 20° and 80° (2θ). Fourier transform infrad red (FTIR) (Perkin Elmer 1600), Raman scattering (Renishaw 2000 Raman spectrometer) and X-ray photoelectron spectroscopy (XPS, ESCALB MK-II, VG Instruments, U.K.), field-emissiong scanning electtron miscroscopy (FE-SEM, FEI Nova 400 Nano), and transmission Electron Microscopy (TEM, Philips CM20).

### Electrochemical properties

Electrochemical measurements were carried out on a CHI 660C instrument with sample (1×1 $cm^2$) as the working electrode, a 2×2 $cm^2$ Pt foil as the counter electrode, and a SCE as the reference electrode. Cyclic voltammetry (CV) was performed between -0.2 and 1 V (*vs*. SCE) at different scanning rates in a 1.0 M HCl aqueous solution at room temperature. The galvanostatic charging/discharging curves were acquired at different current densities between 0 and 0.6 V (*vs*. SCE). Electrochemical impedance spectroscopy (EIS) was conducted at the open circuit potential (OCP) with an AC perturbation voltage of 5 mV. The cycling stability was assessed on the PANI/TiN/PANI electrode supercapacitor using a charge/discharge tester (Land CT2001A, Wuhan LAND Electronics Co., Ltd., China). The two-electrode supercapacitor was assembled symmetrically in a 2032 cell with celgard 2400 as the seperator and 1 M HCl aqueous solution as the electrolyte in the potential range between 0 and 0.6V.

**Electrochemical impedance spectroscopy (EIS)**

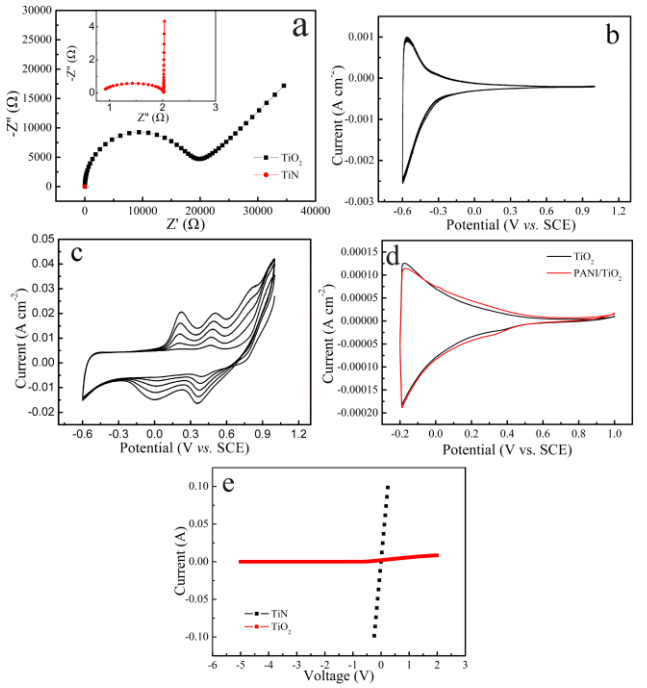


**Fig. S1** (a) EIS plots for $TiO_2$ and TiN NTAs in 1 M HCl by applying AC with an amplitude of 5 mV under open circuit potential conditions. The inset is the amplified EIS plot of TiN-NTAs. Cyclic voltammograms obtained from $TiO_2$ (b) and TiN (c) electrochemically deposited with PANI recorded in a 0.5 M $H_2SO_4$ solution containing 0.05 M aniline for 5 cycles in the potential range of -0.6~1.0V (vs SCE). The scanning rate is 50 mV $s^{-1}$. (d) CV curves of $TiO_2$ before and after PANI polymerization at a scanning rate of 50 mV $s^{-1}$ in 1 M HCl. (e) *I–V* curves of $TiO_2$ and TiN nanotube arrays devices.

Electrochemical impedance spectroscopy (EIS) was performed to determine the conductivity of $TiO_2$-NTAs annealed in air and TiN-NTAs annealed in $NH_3$, as shown in Fig. S1a. Compared to $TiO_2$ (about 20 kΩ), the resistance of TiN decreases by 5 orders of magnitude to below 1 Ω, indicating that TiN has excellent conductivity and is appropriate for aniline monomer electrochemical polymerization. It is also corroborated by the electrochemical deposition curve recorded during the electropolymerizing process as shown in Figs. S1b and c. When $TiO_2$ is used as the working electrode om polymerizing PANI, the CV curves (Fig. S1b) are unchanged even after 5 cycles, suggesting that no reaction has occured. However, when TiN is the working electrode, obvious redox peaks appear from the first cycle in the CV curve (Fig. S1c) and the peak currents keep increasing during the polymerizing process, indicating that aniline has polymerized and the amount of PANI increases with cycle number. Further electrochemical tests reveal that the CV curves are similar before and after polymerization for $TiO_2$-NTAs (Fig. S1d). The results prove that TiN-NTAs is easier to polymerize aniline monomer than $TiO_2$-NTAs due to the higher conductivity of TiN. Since the TiN-NTAs and $TiO_2$-NTAs are fabricated on the Ti foil *in situ*, the electrocal conductivity and sheet resistance of the TiN-NTA and $TiO_2$-NTA are measured from a metal/semiconductor/metal (MSM) structure. The second metal here is the comparative current collector, i.e. Au. Fig. S1e shows the *I-V* characteristics of $TiO_2$ and TiN nanotube array devices. The *I-V* curve of $TiO_2$ NTAs displays a nonlinear and asymmetric behavior. The forward bias from the bottom Ti substrate needs a low turn-on voltage and reverse bias from the top Au electrode needs a relatively high breakdown voltage. This is similar to a Schottky junction with a rectifying behavior and often observed from a semiconductor. The results arise from the semiconducting nature of $TiO_2$. The *I-V* curve of TiN is symmetrical and linear due to the intrinsic metallic conductivity of TiN. The *I–V* curves reveal that TiN has higher electrocal conductivity than $TiO_2$.

**FTIR and Raman scattering**

The FTIR and Raman spectra of TiN and PANI/TiN/PANI NTAs are displayed in Fig. S2. The characteristic peaks of PANI can be observed from Fig. S2a after polymerization. The peaks at 1594 and 1262 $cm^{-1}$ are associated with N=Q=N (Q: quinonoid structure) stretching of the quinoid ring and C-C, respectively. The peaks at 1321 and 1161 $cm^{-1}$ can be attributed to C-N stretching of the secondary aromatic amine and that at 826 $cm^{-1}$ is ascribed to the out-of-plane bending of C-H on the 1, 4-disubstituted ring. Fig. S2b depicts the Raman spectra of TiN and PANI/TiN/PANI. Except the peaks belonging to TiN (353, 526 $cm^{-1}$), the C–C deformation bands of the benzoid ring are found at 1600 and 1563 $cm^{-1}$. The peaks at 1405 and 1347 $cm^{-1}$ are due to $C–N^{\bullet+}$ stretching of delocalized polaronic charge carriers. The benzene C-H bending deformation band at 1179 $cm^{-1}$ is characteristic of the reduced and semiquinone structures. The PANI Raman peaks between 1000 and 300 $cm^{-1}$ show many conformation dependent features. The peaks at 817 and 610 $cm^{-1}$ correspond to two out-of-plane C-H motions and the C–N–C out of plane deformation modes are at 579 and 420 $cm^{-1}$. In short,

Raman and FTIR furnish evidence that the PANI is formed on the TiN-NTAs electrode after electrochemical polymerization.

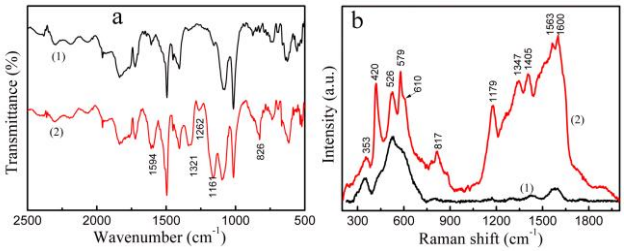


**Fig. S2** FTIR (a) and Raman (b) spectra obtained from TiN (1) and PANI/TiN/PANI (2).

**PANI morphology and loaded quantitites on TiN-NTAs for different electrochemical deposition time**

The FE-SEM images of PANI incorporated into the TiN-NTAs for different depositing time are shown in Fig. S3. When the electrochemical deposition time is 160 s, coaxial PANI/TiN/PANI-NTAs are fabricated as shown in Figs. 2e and f. However, when the polymerization time is increased to 480 s, belt-like structures emerge from the NTAs (Fig.S3a). If the time is further increased to 960 s, PANI nanowires overlapp the NTAs to form a bulk coating (Fig. S3b). The results disclose that the morphology of the PANI/TiN nanocomposites can be adjusted by the deposition time.

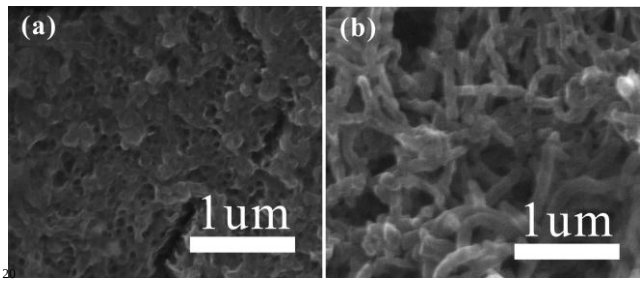


**Fig. S3** SEM inages for PANI/TiN electrochemical deposited in $H_2SO_4$-aniline solution for 480s (a) and 960s (b)

**EDS elemental mapping**

The distribution of PANI on the TiN NTAs is investigated by EDS elemental mapping. Fig. S4 shows that C (referring to as C from PANI) is distributed similarly as Ti (referring to TiN) and N (in both TiN and PANI) around the PANI/TiN/PANI nanotube, indicating that a uniform PANI film is produced on the outer and inner surfaces as well as nanopores of the TiN nanotube walls.

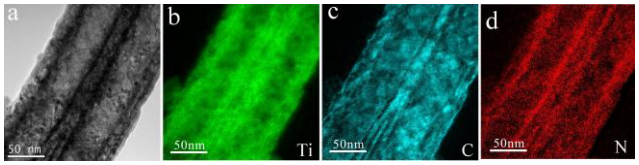


**Fig. S4** Elemental maps of Ti (b), C (c) and N (d) in PANI/TiN/PANI corresponding to the TEM image of (a)

**Gravimetric capacitance as a function of current densities**

Fig. S5 shows the gravimetric capacitance as a function of current densities for the PANI/TiN/PANI electrode determined from the GCD curve in 1 M HCl. The gravimetric capacitance is calculated by the following equation:

$$C = I\Delta t/\Delta E$$

$$C_s = I\Delta t/S\Delta E$$

$$C_m = I\Delta t/m\Delta E.$$

Here, $C$ is the total capacitance, $I$ is the discharge current, $\Delta t$ is the discharging time, $\Delta E$ is the potential window during the discharging process after the inner resistance ($IR$) drop, $C_s$ is the areal capacitance, $C_m$ is the gravimetric capacitance, $S$ is the working area of electrode, and $m$ is the mass incorporated into the PANI. The specific capacitances of the PANI/TiN/PANI elevctrode are calculated to be 1126, 926, 898, 870, 856, 814, and 777 F $g^{-1}$ at current densities of 0.93, 2.3, 4.7, 7.0, 9.3, 23.2, and 46.5 A $g^{-1}$. 70% of the initial capacitance remains when the current density is increased 50 folds from 0.93 to 46.5 A/g, suggesting excellent rate capability. The superior rate capability of the PANI/TiN-NTAs electrode can be attributed to the porous 3D network of the PANI fabricated stably on the TiN nanotube wall as well as high conductivity of both TiN and PANI.

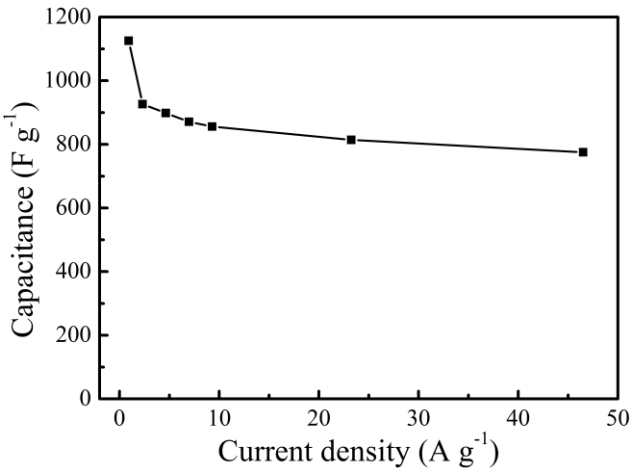


**Fig. S5** Gravimetric capacitance as a function of current density of the PANI/TiN/PANI NTAs electrode.

**Electrochemical capacitive properties of TiN-NTAs incorporated with different amounts of PANI for different electrochemical deposition time**

The CV curves of samples with different amounts of incorporated of PANI at different scanning rates are shown in Fig. S7 a (480s) and b (960s)). In comparation with Fig.3c, the redox peaks in the CV curves in Figs. S7a and 7b are weaker and the shape of anodic and cathodic peaks changes with scanning rates. The charging/discharging curves obtained at current densities of 0.2, 0.5, 1.0, 1.5, 2, and 5 mA $cm^{-2}$ for different depositing time are shown in Fig. S7 (c (480s) and d (960s)), and the corresponding calculated values are displayed in Figs. S7e (480s) and f (960s). For clear comparasion, the areal and gravimetric capacitance of samples with different amounts of loaded PANI as a function of current densities are provided in Fig. S7g and Fig. S7h. For electrochemical polymerization time of 480 s and 960 s, the areal capacitance at a lower current density is higher than that of the 160 s sample (coaxial PANI/TiN/PANI NTAs electrode) because of the larger amount of loaded PANI per $cm^2$. However, when the current density is higher than 5 mA/$cm^2$, the areal capacitance is smaller than that of the PANI/TiN/PANI electrode due to the poorer rate capability. The gravimentric capacitances of TiN-NTAs with diffent amounts of PANI are shown in Fig. S7h. The PANI/TiN/PANI NTAs show the highest gravimentric capacitance for diffent current densities. The results suggest that a large PANI content does not yield better capacitive properties due to the diapppearance of the nanotubular structures. With increasing polymerization, PANI accumulates and overlaps on the surface resulting inmechanical breakdown and tube blocking. Consequently, the specific capacitance decreases drastically when charging/discharging at large scanning rate or big current density because the electrolyte cannot easily access the PANI coated TiN nanotube. The capacitance for large PANI loading is far below the sample deposited for 160 s. The high specific capacitance, excellent rate capability, and good cycling stablility of the sample polymerized for 160 s stem from the high condutivity of the PANI/TiN/PANI and 3D network of PANI on the TiN nanotube. The structure facilitates electrolyte circulation and effective contact with the capacitive PANI thus avoiding mechanical detachment and damage to the PANI structures during the cycling charging/discharging process.

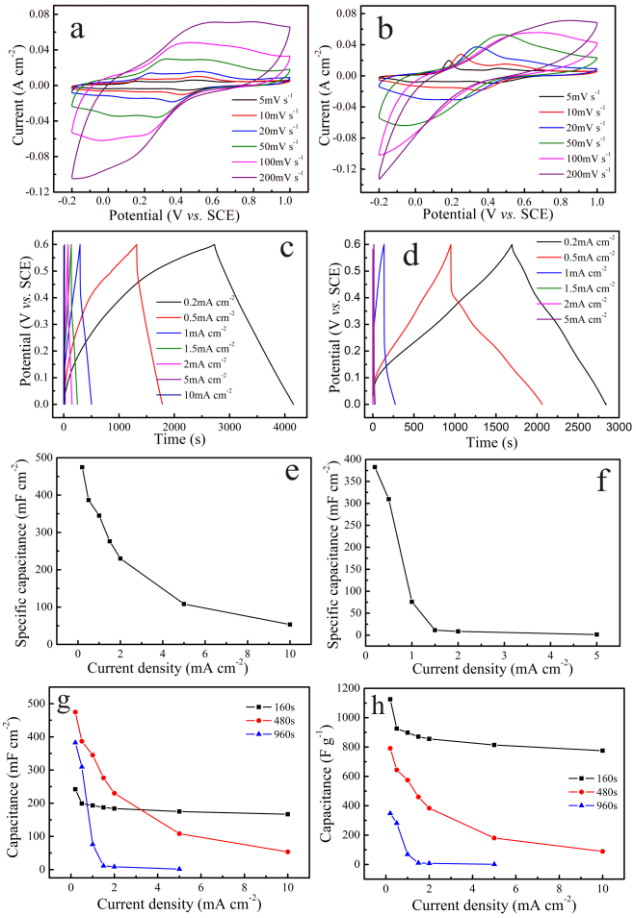


**Fig. S6** CV curves at different scanning rates of 5, 10, 20, 50, 100, and 200 mV $s^{-1}$ obtained from the PANI/TiN electrochemically deposited for 480 s (a) and 960 s (b). Corresponding charge and discharge curves at different current densities of 0.2, 0.5, 1.0, 1.5, 2, and 5 mA $cm^{-2}$ (c) (480s), (d) (960 s). Calculated specific capacitances of PANI/TiN electrochemical lydeposited for 480 s (e) and 960 s (f) at different current densities. Comparison between the areal (g) and gravimetric (h) capacitances at different current densities and diffent PANI loadings is shown.

**Fig. S7 EIS analysis of PANI loaded TiN nanocomposite deposited for different time**

The EIS plots of the TiN and PANI/TiN/PANI electrodes are shown in Fig. S7. Both samples have small interface resistence in 1 M HCl due to the high conductivity of both TiN and PANI. The results demonstrate the excellent rate capability of the PANI/TiN/PANI nanocomposite.

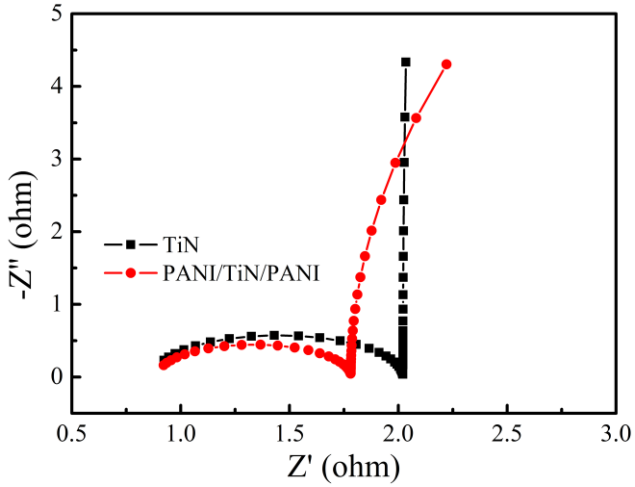


**Fig. S7** EIS analysis of TiN and PANI/TiN/PANI (for 160s polymerization) electrodes in 1M HCl.

**Fig. S8 Electrochemical capacitive properties of electrodes assembled with PANI/TiN/PANI NTAs**

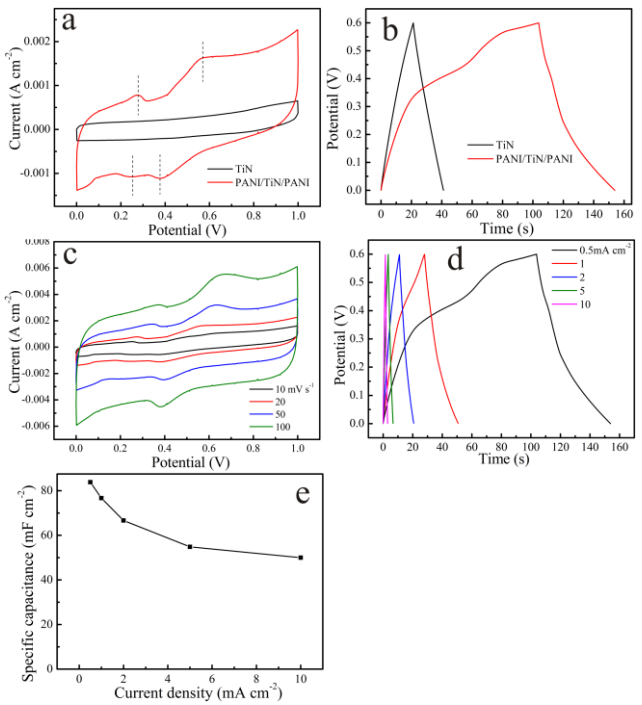


**Fig. S8** (a) CV at a scanning rate of 20 mV $s^{-1}$ and (b) GCD at 0.5 mA $cm^{-2}$ curves of pristine TiN and PANI/TiN/PANI NTAs assembled devices. (c) CV curves with a series of scan rates and (d) GCD curves at different current density of the PANI/TiN/PANI NTAs assembled devices. (e) Areal capacitance as a function of current density of the PANI/TiN/PANI NTAs assembled devices.

Coin-like supercapacitors are constructed based on the symmetric two-electrode structure of the PANI/TiN/PANI-NTAs and the results are shown in Fig S8. The CV curves show two pairs of distinct redox peaks at 0.28/0.22 V and 0.57/0.38 V, which are consistent with the results obtained from the three-electrode configuration. The GCD curves of the two-electrode cell with the PANI/TiN/PANI electrode are shown in Fig. S8b. The areal specific capacitance of one electrode is calculated by the following equation:

$$C_s=2C/S \ , \qquad (1)$$

where $C$ is the measured capacitance of the supercapacitor, $S$ is the area of one composite electrode, and $Cs$ is the specific capacitance based on the electrode area. The calculated areal capacitances of the PANI/TiN/PANI electrode are 88, 77, 67, 55, and 50 mF $cm^{-2}$ at 0.5, 1, 2, 5, and 10 mA $cm^{-2}$, respectively. The specific capacitances of the PANI/TiN/PANI electrode obtained from the three-and two-electrode configuration exhibit a marked difference. The areal capacitance obtained from the three-electrode configuration is larger than that of the two-electrode cell. The bigger values of the former can be understood based on the following analysis. The coin-like supercapacitor is based on the symmetric double PANI/TiN/PANI electrode. When the supercapacitor is charged and discharged, the same active materials work in different potential ranges. The positive electrode operates at a high potential whereas the negative electrode works at a low potential. According to the measurements conducted on the three-electrode configuration (Figs. 3a and 3b), the capacitance of the active materials at low potentials behaves differently from that at high potentials. A value of 147.3 mF $cm^{-2}$ (C1) can be estimated for the potential range between 0 and 0.3 V and has a higher value of 249.8 mF $cm^{-2}$ (C2) between 0.3 and 0.6 V at 0.5 mA $cm^{-2}$. The capacitance of the electrodes decreases with decreasing negative potential. By taking into consideration the equivalent circuit of a two-electrode supercapacitor,


the specific capacitance can be calculated by the following equation:

$$\frac{1}{C}=\frac{1}{C1}+\frac{1}{C2} \ . \qquad (2)$$

According to equation (2), the overall capacitance of the supercapacitor is determined by the smaller of the two components. The overall capacitance is:

$$C = \frac{C1 \times C2}{C1 + C2} = \frac{147.3 \times 249.8}{147.3 + 249.8} = 92.6 \quad (3)$$

The capacitance of 92.6 mF $cm^{-2}$ calcuated from the three-electrode cell is consistent with the experimental value obtained from the two-electrode cell (88 mF $cm^{-2}$). Thus, the results acquired from the three-electrode configuration reported here are reliable. The CV curves (Fig. S8c) obtained at scanning rates of 10, 20, 50, and 100 mV $s^{-1}$ and GCD curves (Fig. S8d) at current densities of 0.5, 1, 2, 5, and 10 mA $cm^{-2}$ reveal that the two-electrode cell based on PANI/TiN/PANI has excellent rate capability.